Influence of lift forces on particle capture on a functionalized surface

Donatien Mottin, Florence Razan, Frédéric Kanoufi, Marie-Caroline Jullien

▶ To cite this version:

HAL Id: hal-03367693

https://hal.science/hal-03367693

Submitted on 27 Oct 2021

Influence of Lift Forces on Particle Capture on a Functionalized Surface

Donatien Mottin,[†,‡] Florence Razan,[‡] Frédéric Kanoufi,[¶] and Marie-Caroline Jullien[*,†]

†*Univ. Rennes 1, CNRS, IPR (Institut de Physique de Rennes) UMR 6251, F-35000 Rennes*

‡*ENS Rennes, SATIE, UMR-CNRS 8029, Campus de Ker Lann, F-35170 Bruz*

¶*Université de Paris, ITODYS, CNRS, UMR 7086, Paris*

E-mail: marie-caroline.jullien@univ-rennes1.fr

Phone: +33 2 23 23 78 52

Abstract

Numerous situations involve the capture of particles onto a functionalized surface in a laminar flow, such as classical biomedical assays, lab on a chip devices or even biological research protocols. Being able to control this capture is thus an important issue that we address in this paper. We focus on a simple and widely used geometry, the straight microfluidic channel, in which particles undergo two weak effects: diffusion towards the functionalized surface and lift forces expelling them away from it. We show that the competition between these two weak mechanisms yields strongly different capture behavior whose ocurence depends on the value of a new lifto-diffusive dimensionless number $\mathcal{N}_{LD}$. We show that tuning the flow rate and the channel dimension to get proper values of this number allow to trigger, via a pure hydrodynamic effect, the capture or non-capture of particles on surfaces. For example, we show that, under

certain conditions, doubling the flow rate reduces the capture rate by four orders of magnitude. Additionally, we provide the particle distribution in the liquid along the channel, resulting from this competition, for different $\mathcal{N}_{LD}$ values. We believe that this work opens new perspectives for analysis and biotechnology applications. More precisely, the proposed model should extend to any transverse force that can be written in the form of a potential energy.

Introduction

The capture of microparticles or nanoparticles onto functionalized surfaces is a critical step in many bioanalysis protocols: nanoparticle tagging [1–4], detection of cancer cells [5–7], or even immunoassays on chip [8–11] . However, the theoretical laws predicting the number of objects that adhere to such surfaces are not specifically designed for particles [12–14], but rather for molecules [15,16]. A major difference between a particle and a molecule, in addition to a lower diffusion coefficient, is that the first one is subjected to flow effects such as lift forces that modifies the particle concentration profile in the cross-section of a channel [17–22]. Neglecting these lift effects obviously leads to a bias in the interpretation of the experimental data.

In this paper, we propose to describe the role of the lift forces in the capture efficiency of microparticles on a functionalized surface. These hydrodynamics forces are generally considered in fluid mechanics occurring at Reynolds numbers $Re = \frac{U_m H}{\nu} > 1$ (where U_m is the maximum liquid velocity, H is the channel height and ν is the liquid kinematic viscosity) [23–25]. These forces result from two mechanisms: the first comes from the shape of the flow, i.e. the shear, which pushes the particles towards the walls [19]; and the second mechanism comes from the particle-wall interaction which tends to move the particles away from the walls [20]. The resultant of these forces leads to a focusing of the particles at specific distances from the walls which have been analyzed theoretically in agreement with experimental and numerical observations [26–29]. However, these lift effects, even weak,

2

may play a role at low Reynolds numbers in straight channels, a geometry commonly used in microfluidic applications. In this paper, we will show that it is the competition between lift forces and diffusion that sets the particle capture efficiency.

By presenting a comprehensive approach, including experiments, numerical simulations and a model, we show that the critical effect of lift forces leads to a reduced capture rate by focusing particles far from the functionalized surface. We introduce a dimensionless parameter that compares the relative importance of diffusion and lift forces, called the Lifto-Diffusive Number $\mathcal{N}_{LD}$, that is the relevant parameter allowing to fully describe the problem.

Using an energetic approach, the particle concentration profile is derived. Based on this knowledge of the concentration profile, we propose a model that predicts the capture rate in term of the $\mathcal{N}_{LD}$ number. This model reproduces the experimental data without any fitting parameters. Two capture regimes are observed. The first regime optimizes particle capture, while in the other one hydrodynamics hides the possible chemical short-range particle-surface interaction and then prevents capture. The actual regime can be modified by changing the value of $\mathcal{N}_{LD}$, which corresponds, for a given channel, to changing the value of the flow rate. Being able to predict and to tune the regime in which an analytical device is operating will be a powerful tool to ensure its efficiency. This can be exploited to either optimize the capture efficiency of particles on sensors or to cancel particle capture.

Experiments

Experimental System

The capture system is sketched on Figure 1: a channel of width $W_c \in [0.5 \, ; 2]$ mm and height $H \in [50 \, ; 75] \, \mu$m, filled with deionized, DI, water, of density $\rho = 10^3$ kg/m^3 and of dynamic viscosity $\eta = 10^{-3}$ Pa s, with $\nu = \eta/\rho$. The microfluidic channel is manufactured using classical soft-lithography and PDMS techniques [30]. The channel is then sealed over the glass slide using a mechanical pressure via a home-made clamping system. An injection flow
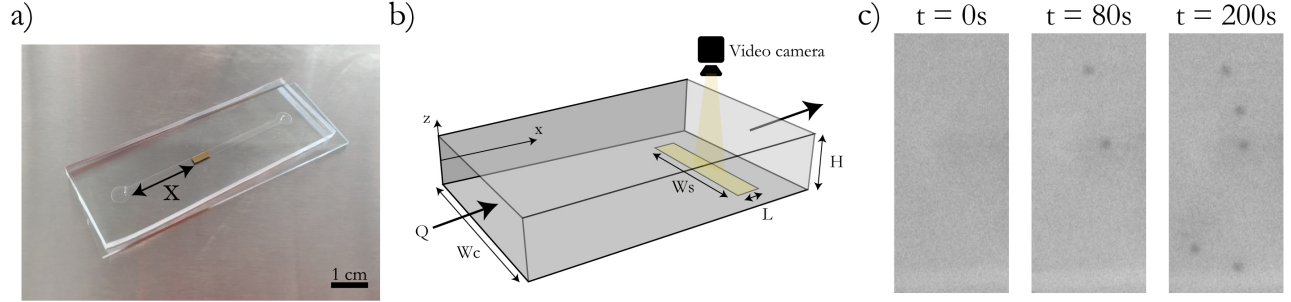
3

Figure 1: (a) Photograph of the microfluidic system. The capture surface is located at a distance x from the channel inlet.(b) Sketch of the experimental system. The channel, of height H and width W_c, contains a functionalized surface of width W_s and length L. The flow is in the x-direction of flow rate Q. (c) Example of images recorded by a video camera set up on a microscope during an experiment. Extraction of a 20 by 45 μm area over time.

rate $Q \in [100; 20,000]\mu$L/h is imposed using a Harvard Apparatus PHD 2000 Infusion syringe pump, resulting in Reynolds number values between $2\,10^{-2}$ and 15, ensuring a laminar flow. Note that for the highest flow rate, the deformation of the cavity is estimated to be lower than 1.5%, this effect will thus be disregarded. DI water is loaded with polystyrene particles of density $\rho_p = 1.03\,10^3$ kg/m^3, diffusion coefficient D and radius $a \in [0.5\,;2.5]\ \mu$m $\ll H$ at a concentration $c_0 \in [5\,10^{12}\,;5\,10^{15}]$ m^{-3} (micromod Partikeltechnologie GmbH), which corresponds to an average inter-particle distance between 8 to 60 diameters. COOH groups are grafted on particles surface, whose deprotonation in water exhibits COO- negative surface charges. The capture surface is obtained by depositing gold (Au) over an area of prescribed size $W_s \times L$ on a glass substrate using conventional microfabrication techniques (Au-Ti PECVD and lift-off). The thickness of the deposited gold layer of 200 nm is much smaller than the thickness of the channel, so that the flow is not disturbed by the sensor surface. The glass slide is then dipped into a 0.2% w/v PolyEthyleneImine aqueous solution (PEI, Sigma-Aldrich) during 2 minutes [14]. A monolayer of PEI auto-assembles on the Au surface, exhibiting positive surface charges [31]. Thus, particles can adhere on the capture surface due to opposite surface charges, guaranteeing that the capture is not limited by any reaction at the surface. The coating ensures that the electrostatic interactions take place only on the capture surface, which has been observed experimentally as no capture events were observed

outside of the gold surface.

NaCl (SigmaAldrich) is added to the solution at a concentration of 10^{-2} M, reducing the electrostatic interactions range to 3 nm [32]. The capture surface is of width $W_s \in [50\,;270]$ μm and length $L \in [50\,;250]$ μm and is located in the middle of the floor of the channel. As $H \ll W_c$ and $W_s < W_c - 2H$, a 1D Poiseuille flow profile over the capture surface is further assumed and corner effects can be disregarded. In a first step, the microfluidic device is filled with DI water. Then, at $t = 0$, the solution containing the particles is injected at a constant flow rate for the whole duration of the capture experiment. The capture of particles on the gold surface is tracked using a Pixelink PL-B625 video camera mounted on a Karl Suss reflective microscope. As light is reflected only on the gold surface, the particles sticking on it appear as black spots on a white background [14]. The number of captured particles N_p with time is thus measured by image treatment with ImageJ [33,34] and the capture rate $J = \frac{dN_p}{dt}$ is inferred.

Experimental Capture of Particles by a Functionalized Surface

A typical experiment consists in counting the number of particles, originally present in a solution of concentration c_0 flowing at a flow rate Q, that adsorb onto a micrometric large Au functionalized surface. The sensing reaction is modelled by the electrostatic interaction which is developped between a COO- terminated PS beads and a PEI, NH3+ terminated, coated Au surface. The experimental capture rate $J = \frac{dN_p}{dt}$, $i.e.$ the number of particles adsorbing on the total capture surface per unit of time, is obtained by performing a linear regression in the stationary state (see Figure 2). Note that the initial behavior of the curve probably comes from a dilution effect. Indeed, at the time of particle injection, the advancing front of the solution containing the particles is subject to the Taylor-Aris dispersion and is most certainly responsible for the initial behavior of the curve. For this reason, we only consider the stationary state and disregard this transient behaviour. Desorption events have not been observed.
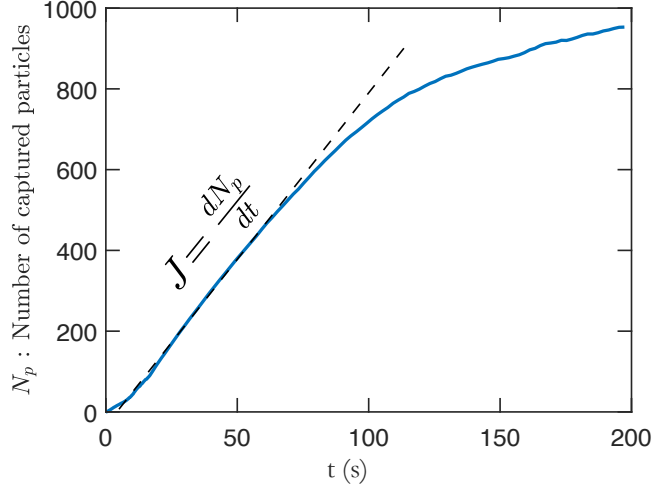
Figure 2: Example of the evolution of the number of captured particles over time. The capture rate J is measured in the stationary regime. The long time signal decay is due to surface saturation.

Figure 3 displays the dimensionless capture rate $\frac{J}{Dc_0 W_s}$ obtained in the experiments as a function of the Péclet number $\text{Pe}_S = \frac{QL^2}{DW_c H^2}$. The Péclet number is used to determine whether a particle convected above the sensor by the flow has time to diffuse towards the sensor. To do this, the Péclet number is built on the ratio between a diffusion time and a convection time. Generally, the diffusion time is taken on the height of the channel, $\tau_D = H^2/D$, and the convection time on the average velocity $\tau_c = H^2 W_c/Q$, giving a Péclet number $\text{Pe}_H \sim Q/DW_c$. In the case we are interested in, $\text{Pe}_H \gg 1$ and only the particles contained in a thin layer of thickness δ_s, called the depletion length, can be captured. It is then necessary to build a new Péclet number, based on this depletion length, that depends upon shear rate and sensor length, $\text{Pe}_S = \frac{QL^2}{DW_c H^2}$ [15]. In a way, this Péclet number defines the range of influence of the sensor, if $\text{Pe}_S < 1$, the depletion thickness is larger than the length of the sensor (diffusion upstream of the sensor can take place) but still smaller than the channel height; on the other hand for $\text{Pe}_S > 1$, this depletion thickness is thinner than the length of the sensor. In our experiments both Pe_H and Pe_s are greater than one, an experimental configuration representative of a large number of experiments in bioassays [35–37].

6

Up to our knowledge, the only universal theory concerns the case of molecule capture which is usually extended to nano and microparticules. Indeed, electrochemists have extensively studied the problem [16,38–43] which has been rationalized by Squires *et al.* [15]. In the framework of this theory, the collection regime for $\mathrm{Pe}_H, \mathrm{Pe}_S \gg 1$ falls into what the authors call the partial collection regime. In this case, the capture rate is given by $J_0 = 1.468 \, Dc_0 W_s \mathrm{Pe}_S^{1/3}$ [16], displayed as a solid line on Figure 3. While part of the experiments seems to be properly described by the convection-diffusion theory, most of the capture rates are way smaller than J_0. In light of this experimental result, additional effects have to be considered as we deal with particles instead of molecules. We address this issue in the following section.
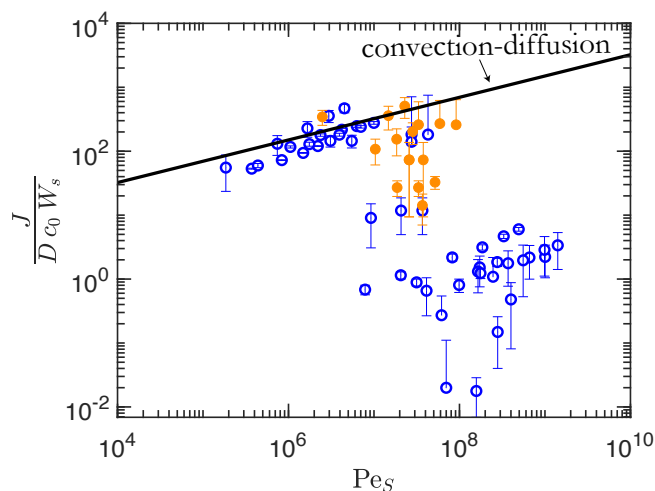

Figure 3: Comparison of experimental results with classical convection-diffusion theory. Dimensionless capture rate $\frac{J}{Dc_0 W_s}$ as a function of the Péclet number Pe_S. (○) Experiments for a capture surface located $x = 5$ mm downstream from the channel inlet, with [NaCl]$=10^{-2}$ M in the particle solution. (●) Experiments for a capture surface located $x = 5$ cm downstream from the channel inlet with no added NaCl in the particle solution. (Black solid line) Theoretical convection-diffusion capture rate J_0 from Amatore *et al.* [16].

Results and Discussion

Relevant Dimensionless Parameters

From a purely hydrodynamic point of view, particles in a Poiseuille flow are submitted to lift forces that develop transversely to the main direction of the object trajectory. Such additional forces, in a laminar flow, have been extensively studied since the first experiments of Segré and Silberberg [17,18]. In their experiments, they injected a suspension of particles in a tube and observed that, at the end of the tube, the particles were all localized on a circle in a cross-section. We suspect these forces to come into play in our experimental system, by moving particles away from the walls of the channel. By emptying the vicinity of the capture surface from particles, lift forces reduce drastically the capture rate. Lift effects emerge due to the inertia of the liquid at finite Reynolds number, leading to a global force pushing the particles towards the walls [19]. Extensive computations show that an additional lift force expels the particle away from the wall [20]. Equilibrium is reached when these two opposite forces are of same magnitude giving rise to the particle focusing at equilibrium positions, in the solution and far from the sensor surface. More formally, Schonberg and Hinch derived a theoretical model [19]. Their approach consists in studying the Poiseuille flow perturbed by the presence of particles. More technically, the authors employ a singular perturbation expansion of the Oseen equation in which the inertial and viscous terms are of the same order of magnitude. The size of the particles is small enough that the perturbation is small, so the convective term can be linearized. The boundary conditions are two parallel plates and an adhesion condition on the particle. Their numerical solution can be fitted by: $v_{z_{\text{Lift}}}(\tilde{z}) = v^*(2.18\,\tilde{z} - 21.23\,\tilde{z}^3) = v^*f(\tilde{z})$ where $\tilde{z} = z/H$, $v^* = \frac{9}{4}\frac{a^3Q^2}{\nu W_c^2 H^4}$ is the characteristic lift velocity, at least for $Re < 15$ above which it shows a slight dependence in Re which we will not discuss. The function $f(\tilde{z}) = 2.18\,\tilde{z} - 21.23\,\tilde{z}^3$ is plotted on Figure 4a and exhibits two stable equilibrium points at $\tilde{z} \simeq \pm0.32$. Consequently, in a system where there is no diffusion, all the particles are laterally displaced by the lift force up to one of these two

8

focusing positions.

The lift force is computed considering that it is balanced by the viscous drag force $6\pi\eta av$:

$$\mathcal{F}_{\text{Lift}} = 6\pi\eta a \, v_{z_{\text{Lift}}}(\tilde{z}) = \mathcal{F}^* f(\tilde{z}) \tag{1}$$

where $\mathcal{F}^* = 6\pi\eta av^* = \frac{27\pi}{2}\frac{a^4\rho Q^2}{H^4 W_c^2}$ is the characteristic lift force amplitude. In order to model the particle distribution on a cross-section of the channel, we propose to give a statistical representation of this distribution. Thus, the potential energy profile created by the lift force at any location $z \in [-H/2, H/2]$ can be computed using $E_p = -\int_0^z \mathcal{F}_{\text{Lift}}(u)\mathrm{d}u = E_p^* \, g(\tilde{z})$ with $E_p^* = \mathcal{F}^* H = \frac{27\pi}{2}\frac{a^4\rho Q^2}{H^3 W_c^2}$ and $g(\tilde{z}) = -\int_0^{\tilde{z}} f(u)\mathrm{d}u = -1.09\,\tilde{z}^2 + 5.31\,\tilde{z}^4$. The shape of this energy, g, is plotted on Figure 4b. Two minima are located at $\tilde{z} = \pm 0.32$ which corresponds to the accumulation points of particles under lift forces focusing.
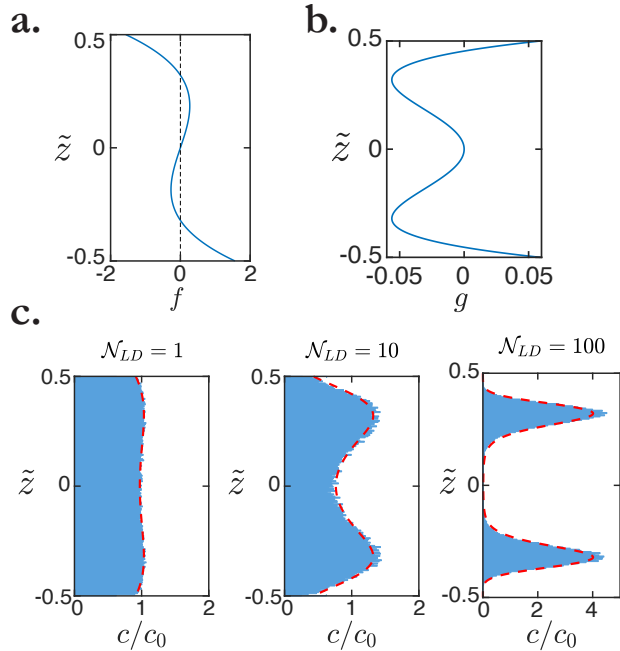

Figure 4: Numerical simulations and analytical models for the particle concentration profile in a channel without capture surface, $\tilde{z} = \frac{z}{H}$ (a) Dimensionless lift velocity function $f(\tilde{z}) = 2.18\tilde{z} - 21.23\tilde{z}^3$. (b) Dimensionless lift potential energy $g(\tilde{z}) = -1.09\tilde{z}^2 + 5.31\tilde{z}^4$. (c) Particle concentration profile $c(\tilde{z})$ at equilibrium for different values of $\mathcal{N}_{LD}$ obtained: (dashed red line) by the analytical theory, and (blue area) by the sequential Lagrangian simulations.

Since a lift effect might be involved, stemming from non-linear effects, the problem would

9

be naturally described in term of Reynolds number $Re = \frac{U_m H}{\nu}$. However, as shown in Figure 5, there is no trend of the capture rate as a function of the Reynolds number.
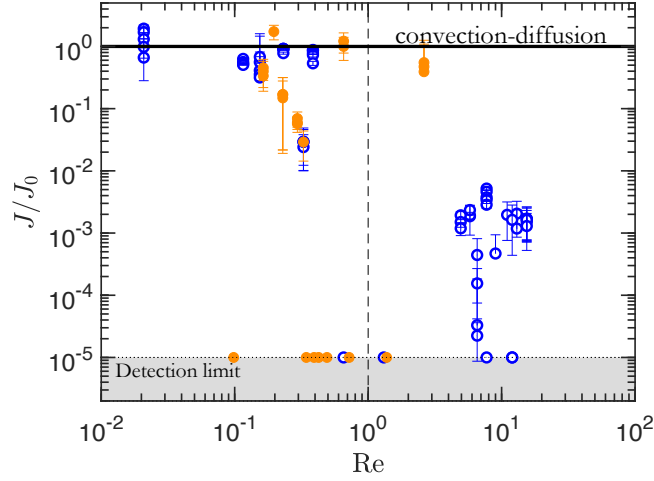

Figure 5: Dimensionless capture rate J/J_0 as a function of the Reynolds number $Re = \frac{U_m H}{\nu}$. ($\circ$) Experiments for a capture surface located $x = 5$ mm downstream from the channel inlet, with [NaCl]$=10^{-2}$ M in the particle solution. ($\bullet$) Experiments for a capture surface located $x = 5$ cm downstream from the channel inlet with no added NaCl in the particle solution. (Black solid line) Theoretical convection-diffusion capture rate from Amatore $et\ al$ [16].

We thus introduce another dimensionless number based on the ratio between the time required for a particle to move up to the focusing localizations $t_{\text{Lift}} \sim H/v^*$ (the time required to deform the concentration profile from a homogeneous to a bimodal one), to the time necessary for a particle to diffuse on the height of the channel $t_{\text{Diff}} \sim H^2/D$ (the time required to recover a homogeneous concentration profile). This number is further called the Lifto-Diffusive Number.

$$\boxed{\mathcal{N}_{LD} = \frac{t_{\text{Diff}}}{t_{\text{Lift}}} = \frac{27\pi}{2k_B T} \frac{Q^2 \rho a^4}{W_c^2 H^3} = \frac{E_p^*}{k_B T}} \tag{2}$$

where k_B is the Boltzmann constant and T is the absolute temperature, which stems from the Einstein formula $D = \frac{k_B T}{6\pi \eta a}$. This number is a Péclet-like number explicitly written in term of the transverse lift velocity.

For $\mathcal{N}_{LD} \ll 1$, diffusion is much faster than the lift focusing and the profile is expected to be homogeneous. Oppositely, for $\mathcal{N}_{LD} \gg 1$, the particles are attracted at the focusing

10

points way faster than they can diffuse out of it. For intermediate values of $\mathcal{N}_{LD}$, both contributions must be taken into account leading to a continuum of concentration profiles between the two extreme cases.

Particle Concentration Profile under Lift Forces

We now turn to the derivation of the equilibrium particle concentration profile under lift forces and diffusion in a channel without considering any capture surface. Particles are considered in a diluted regime, *i.e.* particles do not interact between them, neither from short range electrostatic forces, nor via hydrodynamic interactions. This assumption is checked experimentally by verifying that, for a given set of experimental parameters, the capture rate varies linearly with the particle concentration. A Maxwell-Boltzmann distribution is thus used to predict the equilibrium concentration profile.

This distribution is commonly used to describe the thermodynamic state of a population of objects that do not interact one with each other and are submitted to thermal diffusion, typically used to describe the kinetic theory of gases. In our system, the particles do not interact with each other and are subject to diffusion and lift forces. We make the assumption that this gas of particles in a carrier fluid of viscosity η can be described by this statistic. In this case, the concentration profile $c(\tilde{z})$ results from the competition between the lift energy $E_p(\tilde{z}) = E_p^* g(\tilde{z}) = \mathcal{N}_{LD} k_B T g(\tilde{z})$ and the thermal energy $k_B T$, thus the Maxwell-Boltzmann distribution writes in this framework:

$$c(\tilde{z}) = c_0 \frac{\exp\left(-\frac{E_p(\tilde{z})}{k_B T}\right)}{\int_{-\frac{1}{2}}^{\frac{1}{2}} \exp\left(-\frac{E_p(u)}{k_B T}\right) du} = c_0 \frac{\exp\left(-\mathcal{N}_{LD} \, g(\tilde{z})\right)}{\int_{-\frac{1}{2}}^{\frac{1}{2}} \exp\left(-\mathcal{N}_{LD} g(u)\right) du} \tag{3}$$

As such, the concentration only depends on $\mathcal{N}_{LD}$ and $\tilde{z}$. Figure 4c presents concentration profiles at equilibrium for different $\mathcal{N}_{LD}$ values. For $\mathcal{N}_{LD} \ll 1$ the concentration profile tends to be homogeneous, while for $\mathcal{N}_{LD} \gg 1$ the concentration profile tends to be bi-modal, which is in agreement with the discussion on the significance of the Lifto-Diffusive Number. These

11

results are supported by Lagrangian simulations that agree quantitatively with the analytical model, illustrating the relevance of using the Maxwell-Boltzman distribution. Technical details of these simulations can be found in the supporting information, SI (see section S1). The numerical tool, *LiDi*, that we have developed to obtain these profiles is available at http://lidi.ens-rennes.fr/download. This tool has other functionalities, detailed in SI (see section S2).

Particle Capture Law under Lift Forces

As the concentration profile in a channel without capture surface is now established, we now turn to the prediction of the particle capture law in a channel by introducing a capture surface. In this work, we recall that the capture is not limited by any reaction at the surface.

The reference capture rate $J_0 = 1.468 \, DW_s \text{Pe}_S^{1/3} c_0$ corresponds to a homogeneous concentration profile upstream of the capture sensor. Taking lift into account ($\mathcal{N}_{LD} > 1$), the region near the walls ($\tilde{z} \simeq \pm 1/2$) upstream of the capture surface is depleted from particles. The bulk concentration c_0 thus have to be amended by the actual particle concentration c_1 entering the vicinity of the capture surface, $c_1 = c\left(\tilde{z} = -1/2\right) = \xi c_0$, where :

$$\xi = \frac{c\left(\tilde{z} = -\frac{1}{2}\right)}{c_0} = \frac{\exp\left(-0.059 \, \mathcal{N}_{LD}\right)}{\int_{u=-\frac{1}{2}}^{+\frac{1}{2}} \exp\left(-\mathcal{N}_{LD} g(u)\right) \mathrm{d}u} \tag{4}$$

ξ thus corresponds to a multiplicative factor to the convection-diffusion theory.

$$J = \left(1.468 \, DW_s \text{Pe}_S^{\frac{1}{3}}\right) c_1 = \xi J_0 \tag{5}$$

The experimental results represented as points on Figure 6 present the capture rate ratio J_{exp}/J_0 as a function of $\mathcal{N}_{LD}$, while the model $J/J_0 = \xi$ is sketched as a solid line. Remarkably, the model fits the experimental results without any fitting parameter, showing that the discrepancy from a purely convection-diffusion problem stemming from lift forces

12

is relevant. While in the $\mathcal{N}_{LD} < 1$ the capture rate is stable, making it perfect for classical capture application, in the $\mathcal{N}_{LD} > 1$ region the capture rate falls sharply. For example, simply doubling the flow rate, going from $\mathcal{N}_{LD} = 30$ to $\mathcal{N}_{LD} = 120$, divides the capture rate by 15 000. This abrupt evolution can have dramatic consequences on the capture rate. Experimentally, one can also compute $Q_c = Q(\mathcal{N}_{LD} = 1)$, the critical flow rate above which lift effects appear in a system:

$$Q_c = \sqrt{\frac{2k_B T W_c^2 H^3}{27 \pi \rho a^4}} \tag{6}$$
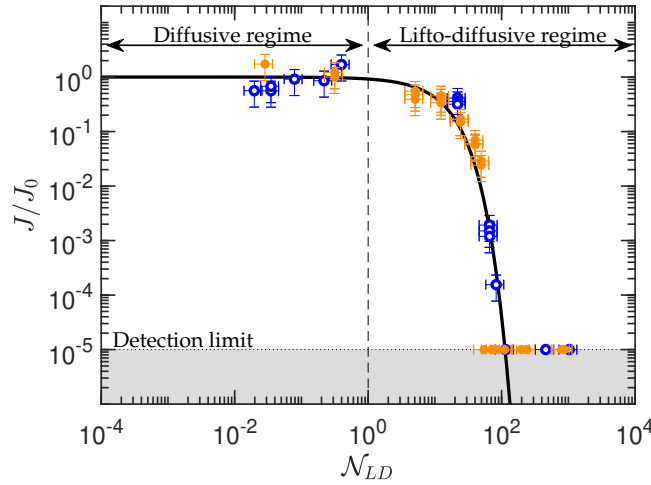

Figure 6: Dimensionless capture rate J/J_0 as a function of the Lifto-Diffusive Number $\mathcal{N}_{LD}$. (Black solid line) Analytical model for ideal non-interacting non-deformable spherical particles in a laminar Poiseuille flow in a rectangular channel. ($\circ$) Experiments for a capture surface located $x = 5$ mm downstream from the channel inlet, with [NaCl]=10^{-2} M in the particle solution. ($\bullet$) Experiments for a capture surface located $x = 5$ cm downstream from the channel inlet with no added NaCl in the particle solution. Experiments with no particle capture are plotted at the detection limit.

Table S1 in SI reports the computed values of ξ as a function of the Lifto-Diffusive Number $\mathcal{N}_{LD}$. For practical issues, for $\mathcal{N}_{LD} \leq 70$, these values can be approximated within 15 % of relative error by:

$$\boxed{\xi \simeq \exp\left(-0.096\,\mathcal{N}_{LD}\right)} \tag{7}$$

13

Transient Regime Analysis

We have so far studied the equilibrium concentration profiles (Figure 4c). However, the concentration profile evolves from a homogeneous profile at the channel inlet, to the equilibrium profile. As the liquid velocity is z-dependent, the corresponding equilibrium distance is also z-dependent [21]. Figure 7 depicts the Lagrangian simulations at different locations along the flow, together with the analytical equilibrium profile. If we consider that the particle depleted zone due to lift forces is located on a distance $h(x)$ from the wall, defined as the lift-induced depletion thickness (sketched on Figure 8), the equilibrium time needed to deplete this zone is typically $t \simeq \frac{h}{v^*}$, where $v^* = \frac{9}{4} \frac{a^3 Q^2}{\nu W_c^2 H^4}$ is the typical transverse lift velocity. During the same time, the particle moves over a typical distance $x = v_x t \simeq \frac{Qh}{W_c H^2} t \simeq \frac{W_c H^2 \nu}{a^3 Q} h^2$. The lift-induced depletion thickness is thus given by:

$$h(x) \simeq \left(\frac{a^3 Q}{W_c H^2 \nu} x \right)^{1/2} \tag{8}$$

Importantly, it is not necessary to reach equilibrium for the theory for particle capture to be valid. Indeed, equation (8) clearly shows that the equilibrium concentration profile near the capture surface ($h \simeq 0$) is reached instantly (theoretically $x \simeq 0$ and experimentally $x \simeq 2a$), consistently with the Lagrangian simulations, see Figure 7. This fundamental property shows that it is not necessary to reach equilibrium for lift effects to affect capture on a surface. From a practical point of view, even if total equilibrium is reached after several tens of centimetres, lifto-diffusive equilibrium near the walls is reached at the channel inlet. The model is therefore valid regardless of the position of the capture surface along the channel.

Short Range Attractive Interactions

The model considers that the particles do not undergo attractive or repulsive interactions. However, it may happen that short range interactions, such as attractive electrostatic ones, come into play and modify the above analysis [32,44,45].
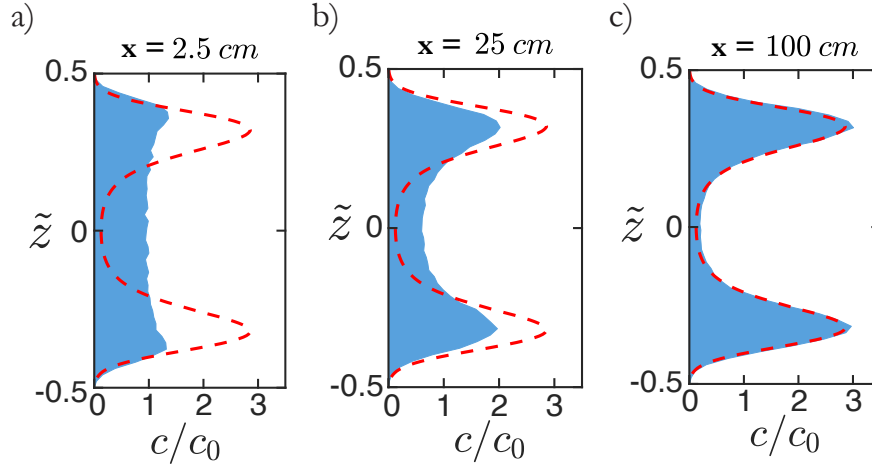
14

Figure 7: Out of equilibrium particle concentration profile for different distances x between capture surface and channel inlet: (a) $x = 2.5$ cm (b) $x = 25$ cm (c) $x = 100$ cm. (blue area) Sequential Lagrangian simulations for $\mathcal{N}_{LD} = 56$, $Q = 5$ μL/min, $a = 500$ nm, $H = 20$ μm and $W_c = 100$ μm. (red dashed line) Equilibrium theoretical profile.

In our experiments, particles are charged negatively and the capture surface is charged positively, thus electrostatic attractive interactions are present. Their amplitude varies with $e^{(-d/\lambda_D)}$ where d is the distance between two charged surfaces and λ_D is called the Debye length [32]. This length varies in water from 1 μm to 1 nm depending on the salt concentration ($\lambda_D \propto c_{\text{salt}}^{-1/2}$), and represents the typical range of electrostatic forces. If, at the beginning of the capture surface, the lift-induced thickness h is smaller than λ_D, as depicted in domain a of Figure 8, the attractive force acts on out-of-equilibrium particles. In such configurations, the lifto-diffusive theory does not apply. The experiments corresponding to this case are plotted as black circles on Figure 9 and the model underestimates the capture rate. To avoid that, one can either place the capture surface further from the inlet thus leaving more time for the lift-induced thickness to propagate (domain c of Figure 8), or add salt to the solution, thus reducing λ_D (domain b of Figure 8). These two cases are successively depicted as blue and orange circle in Figure 3 and fall into the model.
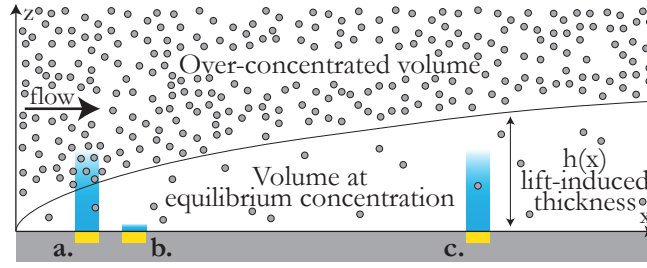
15

Figure 8: Effect of electrostatic interactions on particle capture. The capture surfaces are sketched in yellow. The range of influence of the electrostatic interactions (the Debye length) is in blue. The flow goes from the left to the right. The solid line represents the lift-induced thickness predicted by equation (8): only a ξ fraction of the particles succeeds to diffuse against the lift forces towards the capture surface within this thickness. (a) The range of influence of the electrostatic interaction is larger than the lift-induced thickness. (b-c). Lifto-Diffusive regime. In both cases the lift-induced thickness is thicker than the Debye length, either due to interaction screening by added salt (b) or by locating the capture surface far away from the inlet (c).
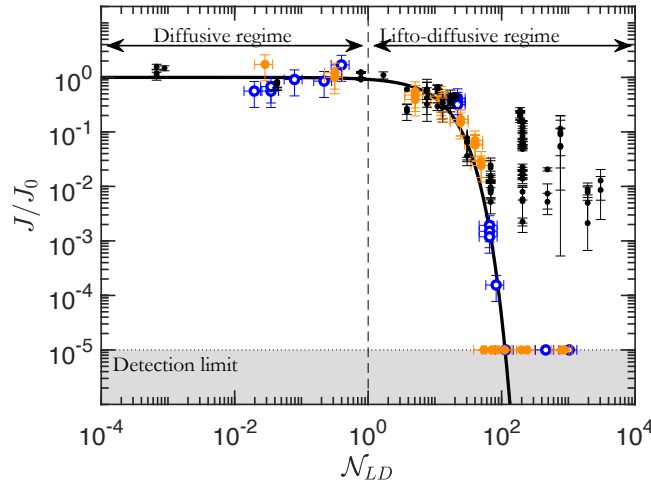

Figure 9: Dimensionless capture rate J/J_0 as a function of the Lifto-Diffusive Number $\mathcal{N}_{LD}$ for all the experiments. It includes experiments captioned in Figure 6 and ($\bullet$) experiments with no added NaCl and with a capture surface only 5 mm away from the inlet, in which the lift-induced thickness is smaller than the Debye length.

Discussion on the capture rate for different values of Pe_H and Pe_s

As stated in the article, our model is only valid for $\text{Pe}_H \gg 1$ and $\text{Pe}_S \gg 1$. For $\text{Pe}_H \ll 1$, diffusion prevails over the whole height of the channel compared to convection. In practice, the flow rate required to reach this regime is so small that the associated $\mathcal{N}_{LD} \ll 1$. We therefore fall back on the $\text{Pe}_H \gg 1$ model for which the capture is complete: $J = QC_0$. On the other hand, if $\text{Pe}_H \gg 1$, as discussed previously in the paper, only the particles contained in the depletion length can be captured and two cases should be considered, depending on the range of influence of the sensor [15]. The case $\text{Pe}_S \gg 1$ is commonly encountered in bioanalysis and corresponds to the present work. The $\text{Pe}_S \ll 1$ case would correspond to very small sensor length (typically below 100 nm) and very low flow rates in order to get such small values of Pe_S. This case is out of scope of this paper.

Conclusions

In this paper, we report a study of particle capture by a functionalized surface for spherical, diluted, non-deformable particles, subject to both diffusion and lift effect in a Poiseuille flow at low Reynolds number. We show that the relevant dimensionless parameter to describe the problem is the Lifto-Diffusive number $\mathcal{N}_{LD}$. The concentration profile reaches an equilibrium profile whose form depends solely on $\mathcal{N}_{LD}$. For $\mathcal{N}_{LD} > 1$, there is a depletion of particles close to the capture surface reducing dramatically the capture rate. Our experimental results are recovered by this model without any adjusting parameter. We believe that this work can have a significant impact on the development of biosensors or analysis lab on chip using micro/nanoparticles. We also believe that this work opens many perspectives for other fields of application of which we provide some tracks below. First, it is legitimate to ask whether this analysis is also applicable to deformable objects or macromolecules for example. For such objects, the difficulty lies in the definition of the lift force which depends strongly on the shape and the deformation of the object, and for which there is not always a consensus as for

example for deformable objects [46–48]. These studies are therefore outside the scope of this study and offer significant prospects for further studies. More generally, this study should extent to any transverse force that can be written in the form of a potential energy (i.e. a force that derives from a position), the theoretical analysis, consisting of equations (1) to (4) can be followed in a similar way considering the transverse force. Finally, this study allows us to consider a new way of sorting the particles using the lift forces in a straight channel. Indeed, this force is to the power of 4 of the particle radius. A factor of 2 on their radius is enough for the lift force to be multiplied by 16. It is therefore quite possible that two populations of particles have very different Lifto-diffusive numbers. In the particular case where one population has a $\mathcal{N}_{LD} > 1$ and the other one a $\mathcal{N}_{LD} > 1$ two different applications can be considered: A first application would be that only the population with $\mathcal{N}_{LD} > 1$ is captured on the surface, the other one being to focus the population with $\mathcal{N}_{LD} > 1$ to recover it specifically thanks to judiciously placing microfluidic outputs.

Acknowledgements

Supporting Information Available

Supporting Information contains technical details on the Lagrangian simulation (S1), Lidi Software User Manual (S2), table values of ξ versus $\mathcal{N}_{LD}$ (table S1) and screenshots from the free-of-access software *Lidi* (figure S1).

References

(1) Ni, K.; Lu, H.; Wang, C.; Black, K. C.; Wei, D.; Ren, Y.; Messersmith, P. B. A novel technique for in situ aggregation of Gluconobacter oxydans using bio-adhesive magnetic nanoparticles. *Biotechnology and bioengineering* **2012**, *109*, 2970–2977.

(2) Guo, H.; Idris, N. M.; Zhang, Y. LRET-based biodetection of DNA release in live cells using surface-modified upconverting fluorescent nanoparticles. *Langmuir* **2011**, *27*, 2854–2860.

(3) van der Maaden, K.; Sliedregt, K.; Kros, A.; Jiskoot, W.; Bouwstra, J. Fluorescent Nanoparticle Adhesion Assay: a Novel Method for Surface p K a Determination of Self-Assembled Monolayers on Silicon Surfaces. *Langmuir* **2012**, *28*, 3403–3411.

(4) Burris, K. P.; Stewart Jr, C. N. Fluorescent nanoparticles: Sensing pathogens and toxins in foods and crops. *Trends in food science & technology* **2012**, *28*, 143–152.

(5) Nunna, B. B.; Mandal, D.; Lee, J. U.; Singh, H.; Zhuang, S.; Misra, D.; Bhuyian, M. N. U.; Lee, E. S. Detection of cancer antigens (CA-125) using gold nano particles on interdigitated electrode-based microfluidic biosensor. *Nano convergence* **2019**, *6*, 1–12.

(6) Tulukguoglu, E.; Bureau, C.; Perez-Toralla, K.; Descroix, S.; Malaquin, L.; Pierga, J.; Bidard, F.; Viovy, J. A microfluidic CTC sorting strategy using self-assembled magnetic particles. Anticancer Research. 2014; pp 6233–6234.

(7) Ferraro, D.; Champ, J.; Teste, B.; Serra, M.; Malaquin, L.; Descroix, S.; de Cremoux, P.; Viovy, J.-L. *Microchip Diagnostics*; Springer, 2017; pp 113–121.

(8) Teste, B.; Malloggi, F.; Siaugue, J.-M.; Varenne, A.; Kanoufi, F.; Descroix, S. Microchip integrating magnetic nanoparticles for allergy diagnosis. *Lab on a Chip* **2011**, *11*, 4207–4213.

(9) Chen, A.; Kozak, D.; Battersby, B. J.; Forrest, R. M.; Scholler, N.; Urban, N.; Trau, M. Antifouling surface layers for improved signal-to-noise of particle-based immunoassays. *Langmuir* **2009**, *25*, 13510–13515.

(10) Teste, B.; Vial, J.; Descroix, S.; Georgelin, T.; Siaugue, J.-M.; Petr, J.; Varenne, A.; Hennion, M.-C. A chemometric approach for optimizing protein covalent immobilization on magnetic core–shell nanoparticles in view of an alternative immunoassay. *Talanta* **2010**, *81*, 1703–1710.

(11) Teste, B.; Kanoufi, F.; Descroix, S.; Poncet, P.; Georgelin, T.; Siaugue, J.-M.; Petr, J.; Varenne, A.; Hennion, M.-C. Kinetic analyses and performance of a colloidal magnetic nanoparticle based immunoassay dedicated to allergy diagnosis. *Analytical and bioanalytical chemistry* **2011**, *400*, 3395–3407.

(12) Kuzmichev, A.; Skolnik, J.; Zybin, A.; Hergenröder, R. Absolute analysis of nanoparticle suspension with surface plasmon microscopy. *Analytical Chemistry* **2018**, *90*, 10732–10737.

(13) Adamczyk, Z.; Siwek, B.; Zembala, M.; Belouschek, P. Kinetics of localized adsorption of colloid particles. *Advances in Colloid and Interface Science* **1994**, *48*, 151–280.

(14) Lemineur, J.-F.; Stockmann, T. J.; Médard, J.; Smadja, C.; Combellas, C.; Kanoufi, F. Optical Nanoimpacts of Dielectric and Metallic Nanoparticles on Gold Surface by Reflectance Microscopy: Adsorption or Bouncing? *Journal of Analysis and Testing* **2019**, *3*, 175–188.

(15) Squires, T. M.; Messinger, R. J.; Manalis, S. R. Making it stick: convection, reaction and diffusion in surface-based biosensors. *Nature Biotechnology* **2008**, *26*, 417.

(16) Amatore, C.; Da Mota, N.; Sella, C.; Thouin, L. Theory and experiments of transport at channel microband electrodes under laminar flows. 1. Steady-state regimes at a single electrode. *Analytical Chemistry* **2007**, *79*, 8502–8510.

20

(17) Segré, G.; Silberberg, A. Behaviour of macroscopic rigid spheres in Poiseuille flow Part 1. Determination of local concentration by statistical analysis of particle passages through crossed light beams. *Journal of Fluid Mechanics* **1962**, *14*, 115–135.

(18) Segré, G.; Silberberg, A. Behaviour of macroscopic rigid spheres in Poiseuille flow Part 2. Experimental results and interpretation. *Journal of Fluid Mechanics* **1962**, *14*, 136–157.

(19) Schonberg, J. A.; Hinch, E. Inertial migration of a sphere in Poiseuille flow. *Journal of Fluid Mechanics* **1989**, *203*, 517–524.

(20) Yahiaoui, S.; Feuillebois, F. Lift on a sphere moving near a wall in a parabolic flow. *Journal of Fluid Mechanics* **2010**, *662*, 447–474.

(21) Matas, J.; Morris, J.; Guazzelli, E. Lateral forces on a sphere. *Oil & Gas Science and Technology* **2004**, *59*, 59–70.

(22) Mutlu, B. R.; Edd, J. F.; Toner, M. Oscillatory inertial focusing in infinite microchannels. *Proceedings of the National Academy of Sciences* **2018**, *115*, 7682–7687.

(23) Callens, N.; Hoyos, M.; Kurowski, P.; Iorio, C. S. Particle sorting in a mini step-split-flow thin channel: influence of hydrodynamic shear on transversal migration. *Analytical chemistry* **2008**, *80*, 4866–4875.

(24) Nieuwstadt, H. A.; Seda, R.; Li, D. S.; Fowlkes, J. B.; Bull, J. L. Microfluidic particle sorting utilizing inertial lift force. *Biomedical microdevices* **2011**, *13*, 97–105.

(25) Zhou, J.; Papautsky, I. Fundamentals of inertial focusing in microchannels. *Lab on a Chip* **2013**, *13*, 1121–1132.

(26) Cherukat, P.; McLaughlin, J. B. The inertial lift on a rigid sphere in a linear shear. *Journal of Fluid Mechanics* **1994**, *263*, 1–18.

(27) Krishnan, G. P.; Leighton Jr, D. T. Inertial lift on a moving sphere in contact with a plane wall in a shear flow. *Physics of Fluids* **1995**, *7*, 2538–2545.

(28) King, M. R.; Leighton, D. T., Jr Measurement of the inertial lift on a moving sphere in contact with a plane wall in a shear flow. *Physics of Fluids* **1997**, *9*, 1248–1255.

(29) Cherukat, P.; McLaughlin, J. B.; Dandy, D. S. A computational study of the inertial lift on a sphere in a linear shear flow field. *International Journal of Multiphase Flow* **1999**, *25*, 15–33.

(30) Xia, Y.; Whitesides, G. M. Soft lithography. *Annual Review of Materials Science* **1998**, *28*, 153–184.

(31) Song, W.-J.; Du, J.-Z.; Sun, T.; Zhang, P.-Z.; Wang, J. Gold nanoparticles capped with polyethyleneimine for enhanced siRNA delivery. *Small* **2010**, *6*, 239–246.

(32) Israelachvili, J. N. *Intermolecular and surface forces*; Academic press, 2011.

(33) Schneider, C. A.; Rasband, W. S.; Eliceiri, K. W. NIH Image to ImageJ: 25 years of image analysis. *Nature Methods* **2012**, *9*, 671.

(34) Rueden, C. T.; Schindelin, J.; Hiner, M. C.; DeZonia, B. E.; Walter, A. E.; Arena, E. T.; Eliceiri, K. W. ImageJ2: ImageJ for the next generation of scientific image data. *BMC bioinformatics* **2017**, *18*, 529.

(35) Zebda, A.; Renaud, L.; Cretin, M.; Innocent, C.; Pichot, F.; Ferrigno, R.; Tingry, S. Electrochemical performance of a glucose/oxygen microfluidic biofuel cell. *Journal of Power Sources* **2009**, *193*, 602–606.

(36) Branagan, S. P.; Contento, N. M.; Bohn, P. W. Enhanced mass transport of electroactive species to annular nanoband electrodes embedded in nanocapillary array membranes. *Journal of the American Chemical Society* **2012**, *134*, 8617–8624.

(37) Sansuk, S.; Bitziou, E.; Joseph, M. B.; Covington, J. A.; Boutelle, M. G.; Unwin, P. R.; Macpherson, J. V. Ultrasensitive detection of dopamine using a carbon nanotube network microfluidic flow electrode. *Analytical chemistry* **2013**, *85*, 163–169.

(38) Newman, J. The Fundamental Principles of Current Distribution and Mass Transport in Electrochemical Cells in Electroanalytical Chemistry, Vol. 6, AJ Bard, ed. *Bard, ed., Marcel Dekher, lnc. New York* **1973**,

(39) Alden, J. A.; Compton, R. G. Hydrodynamic voltammetry with channel microband electrodes: Axial diffusion effects. *Journal of Electroanalytical Chemistry* **1996**, *404*, 27–35.

(40) Compton, R. G.; Fisher, A. C.; Wellington, R. G.; Dobson, P. J.; Leigh, P. A. Hydrodynamic voltammetry with microelectrodes: channel microband electrodes; theory and experiment. *The Journal of Physical Chemistry* **1993**, *97*, 10410–10415.

(41) Ackerberg, R.; Patel, R.; Gupta, S. The heat/mass transfer to a finite strip at small Péclet numbers. *Journal of Fluid Mechanics* **1978**, *86*, 49–65.

(42) Rees, N. V.; Alden, J. A.; Dryfe, R. A.; Coles, B. A.; Compton, R. G. Voltammetry under high mass transport conditions. The high speed channel electrode and heterogeneous kinetics. *The Journal of Physical Chemistry* **1995**, *99*, 14813–14818.

(43) Parant, H.; Muller, G.; Le Mercier, T.; Poulin, P.; Tarascon, J.-M.; Colin, A. Complete study of a millifluidic flow battery using iodide and ferricyanide ions: modeling, effect of the flow and kinetics. *Microfluidics and Nanofluidics* **2017**, *21*, 171.

(44) Hamaker, H. C. The London-van der Waals attraction between spherical particles. *Physica* **1937**, *4*, 1058–1072.

(45) Li, Q.; Rudolph, V.; Peukert, W. London-van der Waals adhesiveness of rough particles. *Powder Technology* **2006**, *161*, 248–255.

(46) Helmy, A.; Barthes-Biesel, D. Migration of a spherical capsule freely suspended in an unbounded parabolic flow. *Journal de Mécanique théorique et appliquée* **1982**, *1*, 859–880.

(47) Singh, R. K.; Li, X.; Sarkar, K. Lateral migration of a capsule in plane shear near a wall. *Journal of Fluid Mechanics* **2014**, *739*, 421–443.

(48) Beaucourt, J.; Biben, T.; Misbah, C. Optimal lift force on vesicles near a compressible substrate. *EPL (Europhysics Letters)* **2004**, *67*, 676.